Relative Impact of Channel Symbol Rate On Transmission Capacity

THOMAS GERARD[1,*], DANIEL SEMRAU[1], ERIC SILLEKENS[1], ADRIAN EDWARDS[2], WAYNE PELOUCH[2], STUART BARNES[2], ROBERT I. KILLEY[1], DOMANIÇ LAVERY[1], POLINA BAYVEL[1], AND LIDIA GALDINO[1]

[1]Optical Networks Group, Department of Electronic and Electrical Engineering, UCL, Torrington Place, London WC1E 7JE, UK
[2]Xtera, Bates House, Church Road, Harold Wood, Essex, UK
*Corresponding author: thomas.gerard.15@ucl.ac.uk

Through C+L band transmission experiments and theoretical modelling, we investigate the impact of channel symbol rate (30, 40, 60, and 85 GBd) on the performance of DCI, metropolitan and core network distances. Two different transponder architectures are investigated: (a) single-carrier receiver and (b) multi-carrier receiver, where multiple subcarriers are received together in a single wideband receiver. Both receivers architectures experience a reduction in the achievable information rate as channel symbol rate increases due to dominating transceiver noise; this holds over all tested transmission distances. However, the multi-carrier receiver shows a weaker performance dependency on symbol rate, as receiver-related impairments dominate. When testing the single-carrier receiver after 630 km we find that by increasing channel symbol rate from 40 to 85 GBd gross capacity decreases by 16%; however, the required number of transceivers to fill the transmission window decreases by 52%. Using the multi-carrier receiver reduces receiver count further. This potentially impacts the cost and complexity of deploying fully-loaded transmission systems.

1. INTRODUCTION

In today's hyper-connected world, it is vital to maximise data throughput while reducing the cost per bit. The cost per bit can be reduced by increasing the channel symbol rate; this maximises the amount of information sent over one channel and, therefore, reduces the number of transceivers required in a given transmission bandwidth. As CMOS technology has evolved, commercial transceiver improvements have increased channel bandwidth from 28 to 66 GBd, and $\geqslant$96 GBd is expected for the next generation of transponders [1].

On the other hand, extensive studies have shown the benefit of using very low symbol rates for nonlinearity mitigation. In [2] it was found that 2.4 GBd is the optimum channel symbol rate for standard single mode fibre systems to minimise nonlinear effects. In [3] a real time record spectral efficiency of 6.21 bit/(s.Hz) over 6,644 km was achieved by using commercial transponders with Nyquist subcarriers at 8 GBd. This holds for ultra-long-haul transmission systems where the system performance is dominated by nonlinear interference noise, imposed by the Kerr effect.

However, to date, no comprehensive analysis have been carried out for short/medium distances, where the system performance is dominated by the transceiver subsystem constrained signal-to-noise ratio (SNR) [4] [5]. In [4], it was experimentally demonstrated, in a back-to-back configuration, that the SNR and achievable information rate (AIR) decreased as the channel symbol rate increased; i.e., the SNR of a DP-256QAM signal decreased from 26 to 18 dB, for an increase in the symbol rate from 15 to 70 GBd, respectively. This upper limit on the achievable SNR in a transceiver subsystem is mainly due to the resolution of the digital-to-analog converter (DAC) and analog to digital converter (ADC). The SNR of an ideal DAC / ADC is defined by the number of bits which sets the quantisation noise floor [6]. In practical converters, other distortion sources will add to this noise floor, leading to an effective number of bits (ENOB) lower than the stated bit resolution. Additionally, mainly due to clock jitter, the ENOB decreases as frequency increases, which consequently diminishes the SNR as the channel symbol rate is increased [7]. It appears, therefore, that increasing channel symbol rate is only beneficial to overall data throughput if it

outweights the associated transceiver-constrained SNR penalty.

As well as ENOB, other noise sources also constrain the transceiver SNR. At the transmitter, the linear amplifiers used to drive the IQ-modulator, as well as the TIA amplifiers used to amplify the received signal, both have an associated noise figure which also typically increases with frequency. Furthermore, non-ideal digital signal processing (DSP) at both the transmitter and receiver has an associated penalty that also constrains the transceiver SNR [8]. A detailed study of the relative impact of transceiver noise vs transmission-related impairments in a high-capacity transmission system can be found in [9], where analysis was carried out on 312x35 GBd channels. However, until now, the impact in performance of using high symbol rate channels compared with low symbol rate channels in such a system has been unexplored.

This paper is an extension of the work presented in [10]. We investigate the symbol rate dependence of transceiver SNR in the context of high capacity short- to mid-distance transmission links. We achieve this by experimentally and theoretically quantifying the impact of transceiver constrained-SNR and channel symbol rate on the performance of data centre interconnection (DCI), metropolitan and core network transmission distances. The trade off between channel performance and cost is further investigated by comparing two receiver architectures: (a) a single-carrier receiver and (b) a multi-carrier receiver, where multiple subcarriers are simultaneously received in a single 126 GHz optical bandwidth receiver.

The remainder of the paper is organised as follows. Section 2 describes the experimental system under investigation: a fully loaded, continuous 90 nm bandwidth transmission window using hybrid Raman-EDFA amplifiers and 70 km fibre spans. Section 3 describes the analytical model used to predict SNR degradation with distance, and includes the parameters needed to apply this model. Section 4 reports our experimental results in four parts. 4.A. measures the back-to-back performance of the single-carrier receiver at different symbol rates. 4.B. reports the back-to-back performance of the multi-carrier receiver and quantifies the variance in subcarrier performance. 4.C. compares transmission results against modelled predictions up to 630 km. Finally, 4.D. reports the achievable information rates of both receiver architectures with distance, and discusses the trade-offs between complexity, performance, capacity and cost.

2. EXPERIMENTAL SYSTEM UNDER INVESTIGATION

The experimental configuration used for this work is shown in Fig. 1. 30, 40, 60 and 85 GBd signals were tested. The multi-level drive signals for 256QAM were generated offline and digitally filtered using a root raised cosine filter with a roll-off of 0.01. Digital pre-emphasis was applied to the signal to compensate for the frequency response of the transmitter components. The resulting in-phase (I) and quadrature (Q) signals for each polarisation were output using four CMOS-based 8 bit DACs with typical 3 dB analog bandwidth at 32 GHz, operating at 92 GSa/s. The signals was subsequently amplified using four linear amplifiers with 55 GHz electrical bandwidth, before being applied to a high bandwidth dual-polarisation (DP) IQ-modulator (from Oclaro). The four carriers were connected to two independent IQ-modulators before being optically amplified to form four Nyquist shaped DP-256QAM signals. The modulated signals were subsequently combined with 90 nm of continuous spectrally-shaped amplified spontaneous emission (SS-ASE) noise [11] [12], used to emulate interfering chan-

nels. A band stop filter (BSF) was used to create a notch within the SS-ASE noise, within which the modulated channels were positioned. Fig. 2(a) illustrates the 4 carriers with all symbol rates considered in this experiment, plus the SS-ASE, covering 11.25 THz of bandwidth.

The transmission link is comprised of a straight-line link of 9 spans, with 70 km of single-mode fibre and hybrid distributed Raman/EDFA amplifier (HRE). In [13], a schematic of the HRE amplifier is illustrated. The HRE provides a continuous gain from 1524.4 nm to 1615.5 nm and used two counter-propagating pumps at 1427 and 1495 nm with output powers of 300 mW and 310 mW into the transmission fibre, delivering a total signal power of 19.5 dBm to the EDFA stage. The single stage EDFA followed by a 90 nm gain flattening filter (GFF), designed to equalise the gain across the entire HRE bandwidth, boosted the signal to a total output power of 22 dBm. As described in detail in [13], each 70 km fibre span is comprised two fibre types; 40 km followed by 30 km with effective core area of 149 μm^2 and 81 μm^2, respectively.

Coherent detection was carried out using a phase- and polarization-diverse coherent receiver incorporating 70 GHz bandwidth photodetectors, and the signal was digitized using a real-time 8 bit oscilloscope with 63 GHz bandwidth, sampling at 160 GSa/s. Digital signal processing was performed as described in [13], which included matched filtering, chromatic dispersion compensation, blind adaptive equalision, frequency offset compensation and decision directed carrier phase estimation.

Two different receiver architectures were investigated: (a) the single-carrier receiver, and (b) the multi-carrier receiver. In (a), only one carrier is received using an intradyne receiver. In this configuration the performance of 30, 40, 60 and 85 GBd channels were tested. For each symbol rate, four carriers with 30.5, 40.5, 60.5 and 85.5 GHz channel spacing were used, respectively. The carrier wavelengths were set such that the second carrier was always at 1552 nm. At the receiver a bandpass filter (BPF) centered on 1552 nm was used to filter out just this carrier (the channel under test). The transmitted spectrum for this test case is illustrated in Fig. 2(a).

In receiver architecture (b), a multi-carrier receiver is investigated by receiving multiple neighbouring channels simultaneously on a single heterodyne receiver with 126 GHz of optical bandwidth [14–16]. In this case the BPF is widened to receive all 126 GHz. Each individual carrier is digitally down converted to baseband before receiver DSP is applied. To fill the receiver bandwidth, three cases are tested: 4×30 GBd, 3×40 GBd and 2×60 GBd, with channels separated by 0.5 GHz in all cases. This receiver configuration is illustrated in Fig. 2(b).

3. ANALYTICAL MODEL

The theoretical analysis of the system under investigation was modelled using the parameters of the experimental system described above. The signal-to-noise ratio was used to estimate the system performance. After chromatic dispersion compensation the SNR$_{\text{Total}}$ can be expressed as

$$\text{SNR}_{\text{Total}} = \frac{P}{\kappa P + N P_{\text{ASE}} + N^{1+\epsilon} \eta P^3},\tag{1}$$

where P is the launch power per channel and N is the number of spans. $\kappa = \frac{1}{\text{SNR}_{\text{TRX}}}$, where SNR$_{\text{TRX}}$ is the maximum SNR that can be achieved in a given transceiver sub-system, and can be measured in a back-to-back configuration. P_{ASE} is the ASE noise power within the channel bandwidth and can be calculated as
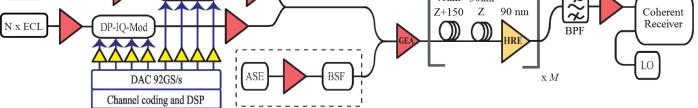
Fig. 1. Experimental configuration. When testing the single-carrier receiver 4 ECL lasers are used at the transmitter. When testing the multi-carrier receiver the number of ECL lasers varies with the symbol rate under test. The local oscillator is set to 1552 nm in all cases. The modulated data channels are co-propagated with 90 nm of SS-ASE noise to emulate a fully loaded C+L band.
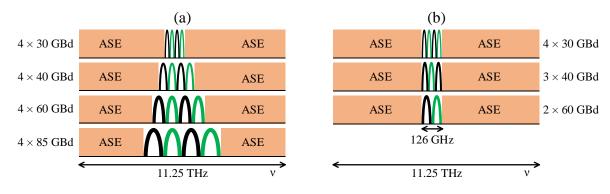

Fig. 2. Transmitted signals for the two receiver architectures under test. In setup (a) the single-carrier receiver is tested by propagating four modulated channels, the second of which is fixed at 1552 nm. Just this channel is optically filtered then digitised. In setup (b) the multi-carrier receiver is tested by receiving 126 GHz of optical bandwidth. Subcarriers are then digitally down converted.

$P_{ASE} \approx GNFh\nu B$, where G is the channel-dependent gain, NF is the effective noise figure, h is the Planck's constant, ν is the channel center frequency and B is the signal bandwidth. In order to estimate the HRE amplifier gain G across the entire 90 nm bandwidth, the frequency dependent signal power profile was calculated by numerically solving the Raman equations [17]. The amplifier NF was experimentally measured and is illustrated in [13] and [9] for the whole spectrum (with an average NF of 1.4 dB). Analysis of G, NF and P_{ASE} and their linear noise contributions to this transmission setup can be found in [9].

The nonlinear interference (NLI) coefficient for one span, η, and the coherence factor, ϵ, were calculated using the inter-channel stimulated Raman scattering (ISRS) Gaussian noise (GN) model [18]. The ISRS GN model accounts for arbitrary, wavelength dependent signal power profiles along fibre spans, which is vital for the modeling of ultra-wideband transmission, particularly for hybrid Raman-amplified links. The application of this model to the transmission system under consideration is described in [9], along with figures illustrating the wavelength dependence of η and ϵ. The extended GN model predicts that the NLI is only weakly dependent on symbol rate for symbol rates $\gtrsim$ 30 GBd [2]. We therefore expect transmission related impairments to affect all the tested symbol rates in this paper (30, 40, 60, 85 GBd) roughly equivalently. It follows that, as transmission distance increases, the performance of all the symbol rates under test should converge (see Eq.1). A modelled prediction of this is illustrated at the end of [9]. Here we seek experimental verification by measuring SNR degradation with distance at 30, 40, 60 and 85 GBd and comparing this to modelled predictions.

4. RESULTS

In this section we used SNR and achievable information rate (AIR) to evaluate system performance. The SNR_{TRX} was evaluated as the ratio between the variance of the transmitted symbols $E[|X|^2]$ and the variance of the noise σ^2, where $\sigma^2 = E[|X - Y|^2]$ and Y represents the received symbols after DSP is applied. The mutual information or AIR was estimated from the received data via Monte Carlo integration and provides an upper bound on the performance for any coded system using DP-mQAM signals [19]. Within [19], it is shown that DP-256QAM is of sufficiently high order to correctly assess the upper bound of AIR for systems with an SNR of 24 dB or less, independent of specific forward error correction (FEC) schemes. As all the SNRs considered here are below this value, we use DP-256QAM throughout this paper without loss of generality.

This section is organised into four subsections. Firstly, the single-carrier receiver architecture is tested in the back-to-back configuration. Secondly, the multi-carrier receiver is tested, also in back-to-back. Thirdly, the transmission results of both architectures are presented alongside the analytical model. Finally, the impact of transceiver architecture and symbol rate on the AIR and overall transmission throughput is evaluated, and the resulting implications on system cost discussed.

A. Single-carrier receiver performance: back-to-back

To evaluate the single-carrier receiver performance, the transmitter was set to the configuration shown in Fig. 2(a). Fig. 3 illustrates the SNR_{TRX} versus the optical signal-to-noise ratio (OSNR) for the channel under test modulated at 30, 60 and 85 GBd, respectively. The experimentally measured SNR_{TRX}
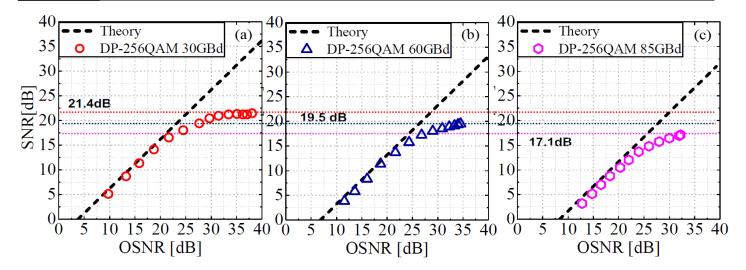
Fig. 3. Single-carrier receiver: Transceiver SNR vs OSNR, measured in a back-to-back configuration for 30 GBd (a), 60 GBd (b) and 85 GBd (c). As symbol rate increases, the maximum achievable SNR and OSNR decreases.

was recorded by connecting the output of the GEA amplifier straight to the BPF filter (see Fig. 1) and then adding ASE noise to the signal to vary the OSNR. The theoretical calculation of OSNR in 0.1 nm of bandwidth is also displayed to provide a performance reference relative to the experimental results. This linear relationship is given by $OSNR = SNR_{TRX_i} + 10\log_{10}(R_s/B)$, where R_s is the symbol rate and B is the noise bandwidth. It can be seen that the highest measured SNR_{TRX} on this back-to-back subsystem was 21.4, 19.5 and 17.1 dB for 30, 60 and 85 GBd, respectively. The primary noise sources that determine SNR_{TRX} are the limited ENOB of the DACs and ADCs, the noise figure from the linear amplifiers used to drive the modulators, and non-ideal digital signal processing (DSP) [4] [5]. It can also be seen that the maximum OSNR achieved by the system decreases as the carrier symbol rate is increased (37.8, 34.5 and 32.0 dB for 30, 60 and 85 GBd, respectively). This is expected behavior: as the same maximum signal power is shared across larger modulation bandwidths the signal power per 0.1 nm of noise bandwidth decreases. This reduction in maximum achievable OSNR consequently impacts the transceiver SNR_{TRX}.

Fig. 4 illustrates SNR_{TRX} for 30, 40, 60, and 85 GBd channel symbol rates. This SNR_{TRX} was measured in a back-to-back configuration without ASE noise loading. Each point in Fig. 4 represents the upper bound in achievable SNR for each symbol rate (for this sub-system). The AIR is also labelled. We observe that as channel symbol rate is increased both the SNR_{TRX} and the AIR decrease. For instance, SNR_{TRX} decreases by 4.3 dB (from 21.4 to 17.1 dB) when the channel symbol rate is increased from 30 GBd to 85 GBd. Similarly, the AIR is observed to drop by 2.7 b/sym for the same change in symbol rate. The drop in transceiver performance can be attributed to the frequency dependency of the transceiver ENOB. Frequency dependent variations in electrical amplifier NF and DSP will also have an effect. Although these absolute values are specific to our system, the principle of this trade off holds generally.

B. Multi-carrier receiver performance: back-to-back

To evaluate the multi-carrier receiver performance, the transmitter was set to the configuration shown in Fig. 2(b). The SNR_{TRX} was measured in the back-to-back configuration without ASE noise loading. Three test cases were considered to ensure an
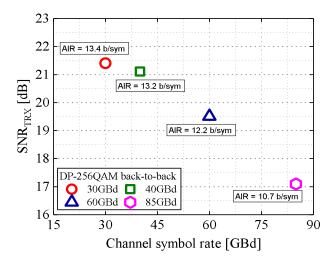

Fig. 4. SNR vs channel symbol rate for the single-carrier receiver, measured in a back to back configuration without noise loading. AIR is calculated for each point by Monte Carlo integration.

aggregate signal bandwidth of 120 GHz: 4 channels × 30 GBd, 3×40 GBd and 2×60 GBd. After reception, the full signal bandwidth was digitised and the SNR of each subcarrier was calculated separately by digitally down converting to baseband. The dependency of each subcarrier's SNR on its frequency offset from the centre of the receiver is shown in Fig. 5. We observe that as subcarriers are received further away from the centre of the receiver's electrical bandwidth the SNR of the subcarrier decreases. This is caused by the decreasing ENOB of the receiver as frequency is increased. Again, these absolute values are specific to our system, though similar penalties will be observed for any receiver whose ENOB decreases with frequency.

Separately from the frequency offset performance dependency, we note that the central 40 GBd channel incurs a 0.9 dB penalty compared to the 40 GBd single carrier receiver, which has decreased from an SNR of 21.4 dB in Fig. 4 to an SNR of 20.5 dB in Fig. 5. This is because the multi-carrier receiver must share the ADC dynamic range among all the incident signal channels. Therefore, the multi-carrier receiver's ENOB per chan-

nel is reduced, impacting all received channels independently of their frequency offset. This absolute receiver penalty is highest for the channels with the lowest symbol rates, as these channels experience the largest proportional reduction in ADC dynamic range per channel.
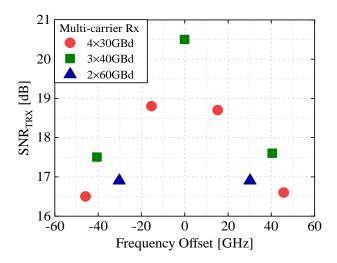

Fig. 5. SNR vs frequency offset from the centre of the multi-carrier receiver. All three test cases occupy the same 120 GHz of optical bandwidth. the SNR of the subcarrier decreases as frequency offset increases, mainly due to the frequency dependency of the receiver's ENOB.

The average SNR_{TRX} for the multi-carrier receiver was calculated by taking the mean of all the subcarrier SNRs in linear units. These are plotted in Fig. 6 against channel symbol rate for the three symbol rates under test. The AIR of each multi-carrier/single-receiver test case is labelled. The SNR_{TRX} of the single-carrier/single-receiver are also displayed for comparison. As before, we observe that as symbol rate increases both SNR_{TRX} and AIR decrease. Both the 30 and 40 GBd results suffer ~3.6 dB penalty when received using the multi-carrier receiver; this penalty is only 2.6 dB for the 60 GBd case. This is because the multi-carrier receiver is dominated by receiver-side impairments, making the transmitter's ENOB-related penalties incurred by increasing the symbol rate less significant.
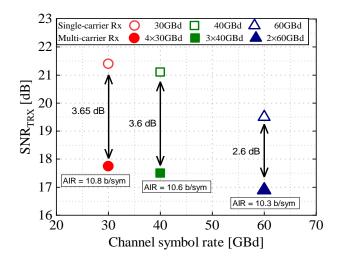

Fig. 6. SNR vs symbol rate for the multi-carrier receiver, in a back-to-back configuration and without ASE noise loading. These results are an average of subcarrier results presented in Fig. 5. Single-carrier results from Fig. 4 are included for comparison.

C. Transmission performance

Here we investigate the impact of transceiver-constrained SNR after optical fibre propagation in a fully loaded C+L band transmission system, when linear noise of the optical amplifier and nonlinear interference noise due to fibre nonlinearity are added to the signal. Fig. 7 illustrates the received SNR_{Total} for each channel symbol rate for the single-carrier receiver, transmitted between 70 and 630 km. The lines are the modelling prediction and the markers are the experimental data (for each experimental result, we report the polarisation average SNR of 4 measurements). After a transmission distance of 210 km the SNR_{Total} decreased by 4.3 dB (from 20.9 dB to 16.6 dB) by increasing the channel symbol rate from 30 GBd to 85 GBd. After increasing the transmission distance to 630 km, the reduction in SNR_{Total} decreased to 3.5 dB (from 19.5 dB to 16.0 dB) for an increase in the channel symbol rate from 30 to 85 GBd. This reduction of the delta SNR (among the different channel symbol rates) with the increase of the transmission distance is because system performance becomes increasingly dominated by amplifier and nonlinear interference (NLI) noise power at longer distances; this diminishes the impact of transceiver SNR_{TRX} on the overall system performance. If the transceiver subsystem was ideal ($SNR_{TRX} = \infty$), the SNR_{Total} would be (approximately) symbol rate independent as the ASE noise power is the same (total power of 22 dBm was maintained for all studied case), and the variation on the NLI noise power is negligible for the studied symbol rates [2]. Therefore, the differences in SNR_{Total} are fully attributed to variations in SNR_{TRX} (see Fig. 4). This is reinforced by the experimental data's agreement with the ISRS GN model, which predicts the performance convergence of the different symbol rates as distance increases.
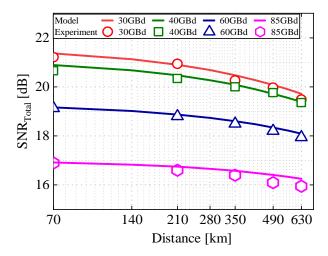

Fig. 7. Single-carrier receiver: SNR vs distance for different channel symbol rates. As distance increases nonlinear noise becomes significant, and hence the SNR gap between high and low baudrates (determined by SNR_{TRX}) decreases.

Fig. 8 illustrates the received SNR_{Total} for the multi-carrier receiver, tested over the same distances as in Fig. 7. Single-carrier receiver data is included in Fig. 8 for comparison. As observed for the single-carrier receiver, the performance of the different symbol rates for the multi-carrier receiver converge with distance. Explicitly, at 70 km the 4×30 GBd result outperforms the 2×60 GBd result by 0.9 dB; this decreases to 0.7 dB by 630 km (a convergence of 0.2 dB). We note that over the same distance the single-carrier receiver suffers a larger penalty: the 30 GBd result outperforms the 60 GBd result by 2.1 dB at 70 km, but

this decreases to 1.5 dB by 630 km (a convergence of 0.6 dB). This comparison shows the multi-carrier performance converges with distance more slowly than the single-carrier. This is because all symbol rates and all receiver types incur similar amounts of linear and NLI from transmission, but the multi-carrier receiver begins with much lower SNR_{TRX}. Therefore the relative effects of the transmission impairments are lower (see Eq. 1).
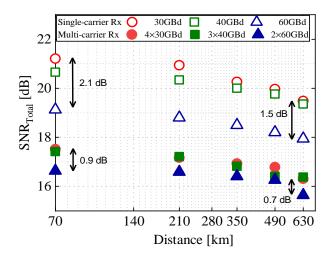

Fig. 8. Multi-carrier receiver: SNR vs distance for different channel symbol rates. Single-carrier receiver results are included for comparsion. Nonlinear interference from transmission closes the performance gap between high and low symbol rates, though more gradually for the multi-carrier receiver.

This is also why the multi-carrier performance decreases more gradually with distance than the single-carrier results. For example, between 70 and 630 km the single-carrier 30 GBd channel drops from 21.2 dB to 19.5 dB (a penalty of 1.7 dB). Over the same distance, the multi-carrier 4×30 GBd channel(s) drops from 17.5 dB to 16.3 dB (a smaller penalty of 1.2 dB). Because the starting SNR_{TRX} of the multi-carrier receiver is lower, the introduction of amplifier noise and NLI has a relatively smaller impact.

D. Achievable Information Rate

Ultimately, in order to quantity the trade-off between transceiver symbol rate and the achievable throughput, Fig. 9 illustrates the single-carrier receiver AIR as a function of distance for each channel symbol rate under investigation. As expected, we see
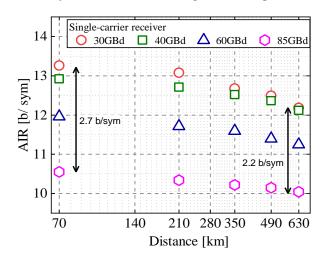

Fig. 9. Single-carrier receiver: AIR over both polarisations as a function of distance. The relative difference between symbol rates decreases with distance.

that the lower the symbol rate, the higher the AIR for any transmission distance. After 70 km, the AIR for 30, 60 and 85 GBd was 13.3, 12.0 and 10.6 b/sym; raising the symbol rate from 30 to 85 GBd therefore incurs a penalty of 2.7 b/sym. After 630 km, the AIR for 30, 60 and 85 GBd was 12.2, 11.2 and 10.0 b/sym respectively; this represents a reduction of 2.2 b/sym caused by increasing the channel symbol rate from 30 to 85 GBd. Therefore, consistent with the results presented in Fig. 8, the delta AIR between best and worst performing symbol rate decreases with distance. As before, this is due to increasing dominance of transmission impairments (which are roughly symbol rate independent) over the transceiver impairments. We note that as transmission distance increases and AIR decreases, lower order modulation formats than DP-256QAM could provide an absolute increase in capacity by achieving a higher $\text{SNR}_{\text{Total}}$. However, for the short- to mid-distances considered here, the relative impact of symbol rate on capacity is applicable to any modulation format capable of a target AIR.
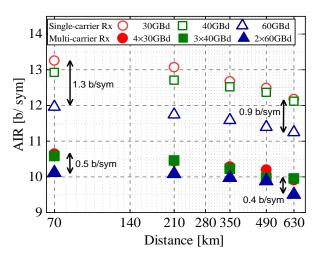

Fig. 10. Multi-carrier receiver: AIR over both polarisations as a function of distance. The relative difference between symbol rates decreases with distance.

The multi-carrier receiver shows a similar trend, though with reduced severity. These results are shown in Fig. 10. Single-carrier results of matching symbol rates are included for comparison. After 70 km, the AIR for 4×30, 3×40 and 2×60 GBd was 10.6, 10.6 and 10.1 b/sym, respectively; raising the symbol rate from 3×40 to 2×60 GBd therefore incurs a penalty of 0.5 b/sym. After 630 km the AIR for the 4×30, 3×40 and 2×60 GBd was 9.91, 9.95 and 9.51 b/sym, respectively; this represents an AIR penalty of 0.4 b/sym incurred by increasing the symbol rate from 3×40 to 2×60 GBd. Therefore, these results also show a reduction in delta AIR with distance (0.1 b/sym). Over the same distances, the single-carrier receiver delta AIR decreases from 1.3 b/sym to 0.9 b/sym.

Comparing the convergence of the signal-carrier AIR from 70 to 630 km (0.4 b/sym) to the multi-carrier convergence (0.1 b/sym), we again observe that the multi-carrier converges more gradually. As with Fig. 8, this is because the receiver-related impairments for the multi-carrier receiver are large, and so transmission impairments have a proportionally lower impact. However, for both the single-carrier receiver and the multi-carrier receiver the conclusion is the same: increasing symbol rate per channel negatively impacts total transmission capacity.

Although it is clear that using a higher symbol rate reduces overall system capacity, it is worth noting that the data rate per

Table 1. Achievable information rates (AIR) after 630 km, and corresponding impact on capacity and transceiver count. These results are specific to the DACs, ADCs, amplifiers and DSP used in this system; however the analysis is applicable to any system where ENOB decreases with frequency.

		Single-carrier				Multi-carrier		
Channel rate	(GBd)	30	40	60	85	4×30	3×40	2×60
AIR @ 630km	(b/sym)	12.2	12.1	11.2	10.0	9.91	9.95	9.51
Capacity/ch	(Gb/s)	365.4	484.4	675.0	853.4	297.3	398.0	570.6
Gross capacity	(Tb/s)	134.8	134.6	125.6	112.6	110.7	110.6	106.1
# Transmitters		369	278	186	132	369	278	186
# Receivers		369	278	186	132	93	93	93

channel does still increase. Similarly, when using a larger signal bandwidth per channel, fewer channels are required to fill a given bandwidth. To illustrate this, Table 1 summarises the transceiver count and channel bit rate for the system tested in this paper using the AIR results after 630 km of transmission. The capacity per channel is obtained by multiplying the AIR by the channel bandwidth, while the transceiver count is calculated by considering the number of channels (with 0.5 GHz spacing) needed to fill this system's 11.25 THz of bandwidth. This information can extended to estimate the cost-per-bit for given transceiver costs. For example, from this data we can see that the single-carrier 85 GBd system achieves 84% of the gross capacity compared to the 40 GBd channel while using only 47% of the transceivers. This is even more apparent when using the multi-carrier receiver, which reduces the required number of receivers by 66% compared to the single-carrier 40 GBd transceiver (though with a higher required electrical bandwidth). These results are specific to the DACs, ADCs, amplifiers and DSP used in this system; however the analysis is applicable to any system where ENOB decreases with frequency. Overall, the results presented in this paper show that when aiming to minimize cost per bit a system designer must balance the transceiver count with the relative reduction in overall bit rate, as well as the cost per transceiver.

5. CONCLUSION

Through experiments and theoretical calculation we studied the reduction in achievable information rate caused by increasing the transceiver symbol rate for regional DCI, metropolitan and core network transmission distances. Two receiver architectures were investigated: (a) a single-carrier receiver and (b) a multi-carrier receiver. In both cases, due mainly to the reduction of transceiver ENOB with frequency, lower transceiver symbol rates enabled a significant increase in overall data throughput. This was observed to hold across 630 km of transmission, with the experimental performance degradation agreeing with the ISRS GN-model. However, this gain in AIR comes with an increase in the number of transceivers required to maximise the use of any given transmission bandwidth. For the 630 km transmission system investigated, 85 GBd signals would require 52% fewer transceivers than the 40 GBd transmission case, and deliver higher data rates per channel. However, it comes with the disadvantage of reducing the total transmission system capacity, as the AIR reduces by 2.1 b/sym with the increasing in the channel symbol rate. The performance impact of using higher symbol rates decreased with distance as linear and nonlinear transmission noise was introduced. This effect was less apparent for the multi-carrier receiver, which was dominated by ENOB-related transceiver impairments.

REFERENCES

1. T. Drenski and J.C. Rasmussen, "ADC & DAC - Technology Trends and Steps to Overcome Current Limitations", *Optical Fiber Communications Conference*, (San Diego, 2018) p. M2C.1.
2. P. Poggiolini, A. Nespola, Y. Jiang, et al.: "Analytical and Experimental Results on System Maximum Reach Increase Through Symbol Rate Optimization," Journal of Lightwave Technology, **34**(8), pp 1872-1885 (2016).
3. S. Grubb, P. Mertz, A. Kumpera, et al., "Real-Time 16QAM Transatlantic Record Spectral Efficiency of 6.21 b/s/hz Enabling 26.2 Tbps Capacity," in *Optical Fiber Communication Conference*, (San Diego, 2018), p. W1B.4.
4. L. Galdino, D. Lavery, Z. Liu, et al., "The Trade-off Between Transceiver Capacity and Symbol rate," *Optical Fiber Communication Conference*, (Los Angeles, 2018), p. M2E.6.
5. L. Galdino, D. Semrau, D. Lavery, et al., "Impact of Transceiver Subsystem on High-Capacity Optical Transmission," *Signal Processing in Photonic Communications*, (Sweden, 2019), p. SpTh2G.1.
6. C. Laperle and M. Sullivan, "Advances in high-speed DACs, ADCs, and DSP for optical coherent transceivers," Journal of Lightwave Technology, **34**(4), pp 629-643 (2014).
7. S. Varughese, J. Langston, V. Thomas, et al., "Frequency Dependent ENoB Requirements for M-QAM Optical Links: An Analysis Using an Improved Digital to Analog Converter Model", Journal of Lightwave Technology, **36**(18), pp 4082-4089 (2018).
8. R. Maher, M. Torbatian, S. Koenig, et al., "Constellation shaping for high symbol rate SNR limited transceivers", *Proc. SPIE 10947, Next-Generation Optical Communication*, (San Francisco, 2019).

9. L. Galdino, D. Semrau, M. Ionescu, et al., "Study on the Impact of Nonlinearity and Noise on the Performance of High-Capacity Broadband Hybrid Raman-EDFA Amplified System," Journal of Lightwave Technology, [Early Access], (2019), DOI:10.1109/JLT.2019.2933246.

10. L. Galdino, D. Semrau, and P. Bayvel, "Candidate Technologies for High-Capacity Optical Communication Systems", *Advanced Photonics Congress*, (San Francisco, 2019), p. NeT3D.1.

11. J.-X. Cai, , Y. Hu, A. Turukhin, et al., "On the Effects of Transmitter Induced Channel Correlation in Broadband WDM Transmission," *Optical Fiber Communication Conference*, (Los Angeles, 2018), p. Th1C.1.

12. D.J. Elson, G. Saavedra, K. Shi, et al., "Investigation of bandwidth loading in optical fibre transmission using amplified spontaneous emission noise," Optics Express, **25**(16), pp 19529-19537, (2017).

13. M. Ionescu, L. Galdino, A. Edwards, et al.: "90 nm C + L Hybrid Distributed Raman/Erbium-Doped amplifier for High Capacity Subsea Transmission", *European Conference on Optical Communication*, (Rome, 2018), p. Mo4G.

14. R. Rios-Müller, J. Renaudier, P. Brindel, et al., "Experimental Comparison between Super-channel and Sub-band Single-Carrier for 400 Gb/s and 800 Gb/s Transport", *European Conference on Optical Communication*, (Valencia, 2015), p. Tu.1.4.4.

15. T. Richter, C. Schmidt-Langhorst, R. Elschner, et al., "Distributed 1-Tb/s all-optical aggregation capacity in 125-GHz optical bandwidth by frequency conversion in fiber", *European Conference on Optical Communication*, (Valencia, 2015), PDP 2.5.

16. D. Millar, R. Maher, D. Lavery, et al., "Design of a 1 Tb/s Superchannel Coherent Receiver", Journal of Lightwave Technology, **34**(6), pp 1453-1463 (2016).

17. S. Tariq, J.C. Palais: "A computer model of non-dispersion-limited stimulated Raman scattering in optical fiber multiple-channel communications," Journal of Lightwave Technology **11**(12), pp 1914-1924, (1993).

18. D. Semrau, R. Killey and P. Bayvel, "The Gaussian Noise Mode in the Presence of Inter-Channel Stimulated Raman Scattering," Journal of Lightwave Technology, **36**(14), pp 3046-3055, (2018).

19. R. Maher, A. Alvarado, D. Lavery, et al., "Increasing the information rates of optical communications via coded modulation: a study of transceiver performance," Scientific Reports, **6**, 21278, (2016).